Published in Image Processing On Line on 2025–12–28.
Submitted on 2025–02–22, accepted on 2025–06–19.
ISSN 2105–1232 © 2025 IPOL & the authors CC–BY–NC–SA
This article is available online with supplementary materials,
software, datasets and online demo at
https://doi.org/10.5201/ipol.2025.602

# A Brief Analysis of the Change Detector by Kervrann et al.

Tristan Dagobert[1], Jean-Michel Morel[2], Gabriele Facciolo[1]

[1]Université Paris-Saclay, ENS Paris-Saclay, Centre Borelli, Gif-sur-Yvette, France
{tristan.dagobert, gabriele.facciolo}@ens-paris-saclay.fr
[2]City University of Hong Kong, Department of Mathematics, Hong Kong
jeamorel@city.edu.hk

*Communicated by* Xavier Bou *Demo edited by* Tristan Dagobert

**Abstract**

This work describes the symmetric method by Kervrann et al. for change detection. The algorithm processes a pair of images using a hypothesis testing technique with an a contrario approach. We perform a brief analysis of the results produced by the method and evaluate its quality and limitations on the Sentinel-2 OSCD dataset.

**Source Code**

The source code and documentation for this algorithm are available on the web page of this article[1]. Usage instructions are included in the `README.txt` file of the archive. The code is a symmetric version of the method from Kervrann et al.

**Keywords:** remote sensing; change detection; hypothesis testing

## 1 Introduction

Change detection is a classic problem in computer vision and notably in the context of spatial remote sensing, where recurrent views of the same scene are taken by Earth observation satellites. This technique has numerous applications in the observation and surveillance of urban development (e.g. [8], [9]), agricultural land exploitation (e.g. [13], [11]), the prediction of natural disasters (e.g. [2], [1]), etc. In this context, change detection relies mainly on the comparison of images taken between two dates. In recent years, supervised deep learning has achieved remarkable results on this problem, see Jiang et al. [10], Cheng et al. [6], and Wu et al. [14]. In this study, we are interested in the approach proposed by Kervrann et al. [12]. This unsupervised change detection method has the advantage of being agnostic to the training data, therefore independent of the satellite, and allowing a priori control of the number of false alarms (a similar approach was proposed in [3]). Although this type of algorithm does not have semantic power, it should be considered as the first step in a processing chain that would employ, in a second stage, specialized semantic classifiers trained on labeled data and focusing on the detected regions.

[1]https://doi.org/10.5201/ipol.2025.602

| | |
|---|---|
| $\phi_{uv}$ | The dissimilarity measure between the patches of $u$ and $v$. |
| $\varepsilon$ | The number of false alarms threshold. |
| $b$ | The square neighborhood around $\mathbf{x}$. |
| $B$ | The square search window related to $\mathbf{x}$. |
| $S$ | The number of scales. |

Table 1: Table summarizing the parameters of the proposed method.

# 2 Algorithm Description

The algorithm under scrutiny [12] was originally designed for change detection in video surveillance. In this context, its design was guided by the requirements for robustness to illumination changes and camera vibration, and for false alarm control. The method is patch-based and multiscale and estimates the change between two grayscale images $u$ and $v$ defined on the same discrete domain $\Omega$, where $u$ is considered as the reference image. Pixel positions are denoted by $\mathbf{x} = (x_1, x_2)^\top \in \Omega$. The parameters of the method described below are summarized in Table 1, while its pseudo-code is shown in Algorithm 1.

**Detection framework.** We introduce a dissimilarity measure $\phi_{uv}(\mathbf{x}, \mathbf{y}, s)$ between two windowed patches $W_s$ of $u$ and $v$, centered at $\mathbf{x}$ and $\mathbf{y}$, respectively, where $s$ is a scale parameter. Its general expression is

$$\phi_{uv}(\mathbf{x}, \mathbf{y}, s) = \sum_{\mathbf{t} \in W_s} g(u(\mathbf{x} + \mathbf{t}), v(\mathbf{y} + \mathbf{t})), \tag{1}$$

where $g : \mathbb{R} \to \mathbb{R}^+$ is a distance function and $W_s$ is a square window of side $2s + 1$. Kervrann et al. consider various possible functions $g$ whose desired properties mainly address the robustness to changes in illumination (see [12, eq. (2.2) to (2.8)]). To ensure some stability, a collaborative neighborhood-wise decision is computed from a fusion rule. It consists of counting the total number of positive decisions denoted by

$$F_s(\mathbf{x}) = \sum_{\mathbf{y} \in B(\mathbf{x})} \mathbb{1}(\phi_{uv}(\mathbf{x}, \mathbf{y}, s) \geq \tau_{u,s}(\mathbf{x})), \tag{2}$$

where $\mathbb{1}(\cdot)$ is the indicator function, $B(\mathbf{x})$ is a square search window centered at $\mathbf{x}$ and $\tau_{u,s}$ is a spatially-varying threshold defined by

$$\begin{aligned} \tau_{u,s}(\mathbf{x}) &= \max(\max_{\mathbf{y} \in b(\mathbf{x}) \setminus \{\mathbf{x}\}} \phi_{uu}(\mathbf{x}, \mathbf{y}, s), \theta_{u,s}), \\ \theta_{u,s} &= \frac{1}{|\Omega|} \sum_{\mathbf{x} \in \Omega} \min_{\mathbf{y} \in b(\mathbf{x}) \setminus \{\mathbf{x}\}} \phi_{uu}(\mathbf{x}, \mathbf{y}, s). \end{aligned} \tag{3}$$

The formulation of (3) is justified as follows. On the one hand, the set $b(\mathbf{x})$ corresponds to a small neighborhood (e.g. $3 \times 3$ pixels) around $\mathbf{x}$ taking into account the possible vibrations of the camera. The values $\phi_{uu}(\mathbf{x}, \mathbf{y}, s)$ of the patches calculated in $b(\mathbf{x}) \setminus \{\mathbf{x}\}$ are assumed to correspond to slightly noisy values of the patch centered at $\mathbf{x}$. The size of this neighborhood $b(\mathbf{x})$ is linked to the amplitude of the image jitter. On the other hand, the term $\tau_{u,s}(\mathbf{x})$ takes the maximum of two bounding values. The first one, $\max_{\mathbf{y} \in b(\mathbf{x}) \setminus \{\mathbf{x}\}} \phi_{uu}(\mathbf{x}, \mathbf{y}, s)$, corresponds to the maximum value calculated in a neighborhood of $\mathbf{x}$ in the reference image $u$. Obviously, the fact that this value is exceeded by $\phi_{uv}(\mathbf{x}, \mathbf{y}, s)$ can reflect a local change between images $u$ and $v$. The second term, $\theta_{u,s}$, is defined as the average of the

smallest distance calculated in the image domain $\Omega$. It ensures that in the case where both images $u$ and $v$ are in a low signal-to-noise ratio regime (e.g. low luminosity), the fact that $\phi_{uv}(\mathbf{x}, \mathbf{y}, s)$ exceeds the threshold $\tau_{u,s}(\mathbf{x})$ would indeed be due to a significant change, and not to a large noise difference between $u$ and $v$. Note that in the original paper, the window sizes of $b(\mathbf{x})$ and $B(\mathbf{x})$ are both 3. However, there is no particular relationship between them, as they address two distinct tasks. Their values can therefore be chosen independently.

A second very restrictive binary decision function $D_s$ is used. It requests the meaningful changes being observable in all the neighborhood $B(\mathbf{x})$ to be set to 1:

$$D_s(\mathbf{x}, B) = \mathbb{1}(F_s(\mathbf{x}) = |B(\mathbf{x})|). \tag{4}$$

**Statistical framework.** One of the main goals proposed by Kervrann et al. is controlling the false alarms rate. To this end, they formulate the change detection problem as hypothesis testing in a statistical framework. The authors first analyze a theoretical formulation of the detection problem assuming a parametric image model containing Gaussian additive noise. However, Kervrann et al. conclude that this modeling would make it difficult to estimate the probability densities of changes or to detect insignificant changes [12, §2.3]. In addition, the authors experimentally observe in several scenes that the empirical distributions of the values $\phi_{uu}$ and $\phi_{uv}$ are highly similar. For these reasons, Kervrann et al. establish an empirical statistical model with no prior on the distribution of changes.

A null hypothesis $H_0$ is introduced, which states that patches from $u$ and $v$ centered at the same location are similar. The authors first define the empirical probability that $|B(\mathbf{x})|$ positive detections occur under the $H_0$ hypothesis as

$$P_{fa}(\mathbf{x}, B, s) \triangleq \mathbb{P}(F_s(\mathbf{x}) = |B(\mathbf{x})| \,|H_0). \tag{5}$$

It is proved that this probability of false alarms can be bounded, thanks to Markov's inequality, as

$$P_{fa}(\mathbf{x}, B, s) \leq \mathbb{E}(\exp(F_s(\mathbf{x}) - |B(\mathbf{x})|)). \tag{6}$$

In order to make local detection more robust, the authors then apply a multiscale strategy to the problem by considering the combination of $S$ windows $(W_s)_{1 \leq s \leq S}$; the size of these windows vary while $B(\mathbf{x})$ remains constant. Although the nested neighborhoods $W_s$ share pixels, Kervrann et al. consider this overlap to be small, and define the variable $\sum_{s=1}^{S} D_s$ as a sum of weakly dependent random variables following a Bernoulli distribution. This assumption allows them to apply Chen's theorem [5], stating that the sum of weakly dependent random variables can be approximated by a Poisson distribution. From definitions (4) and (5) it follows that $\mathbb{E}(D_s|H_0) = P_{fa}(\mathbf{x}, B, s)$. Hence the Poisson law parameter can be expressed by

$$\lambda(\mathbf{x}, B) = \sum_{s=1}^{S} P_{fa}(\mathbf{x}, |B(\mathbf{x})|, s). \tag{7}$$

The probability of false alarms of the multiscale approach is then defined by

$$P_{FA}(\mathbf{x}, S) \triangleq \mathbb{P}\left(\sum_{s=1}^{S} D_s(\mathbf{x}) > k_D(\mathbf{x}) | H_0\right) = 1 - \sum_{k=0}^{k_D(\mathbf{x})} \lambda^k(\mathbf{x}, B) \frac{e^{-\lambda(\mathbf{x}, B)}}{k!}, \tag{8}$$

where "$(k_D(\mathbf{x}) + 1)$ is the actual number of changes (positive decisions) detected for the $S$ different patch sizes at location $\mathbf{x}$"[12, §4.2].

To take into account the long-range information contained in the entire images, Kervrann et al. extend the neighborhood $\mathcal{V}(\mathbf{x})$ up to $\Omega$ so that $P_{fa}$ does not depend on $\mathbf{x}$ anymore. Moreover, they approximate $P_{fa}$ by its majorant found in (6). This yields

$$P_{fa}(s) = \frac{1}{|\Omega|} \sum_{\mathbf{x} \in \Omega} \exp(F_s(\mathbf{x}) - |B(\mathbf{x})|). \tag{9}$$

It follows that the tail of the Poisson distribution is estimated as

$$P_{FA}(\mathbf{x}, F) = 1 - \sum_{k=0}^{k_D(\mathbf{x})} \lambda^k \frac{e^{-\lambda}}{k!}, \tag{10}$$

where

$$\lambda = \frac{1}{|\Omega|} \sum_{s=1}^{S} \sum_{\mathbf{x} \in \Omega} \exp(F_s(\mathbf{x}) - |B(\mathbf{x})|). \tag{11}$$

In order to detect the meaningful changes and control the number of false alarms, the authors adopt the Bonferroni strategy for multiple tests. The authors then define the uniform threshold

$$\alpha = \max\left(\frac{\varepsilon}{|\Omega|}, \inf_{\mathbf{x} \in \Omega} P_{FA}(\mathbf{x}, F)\right), \tag{12}$$

which they prove to imply that the expected number of false alarms in $\Omega$ is lower than the user-defined term $\varepsilon$ [12, Prop. 4.2]. The value $\varepsilon$ is set to 1, meaning that about 1 pixel on average is falsely detected. Finally, the multiscale change detection map $H_\varepsilon(u, v) : \Omega \to \{0, 1\}$ is defined as

$$H_\varepsilon(u, v)(\mathbf{x}) = \mathbb{1}(P_{FA}(\mathbf{x}, F) \leq \alpha). \tag{13}$$

**Symmetrization of the problem.** As the threshold $\tau_{u,s}(\mathbf{x})$ introduced in (3) depends on the image $u$, the change detection map between the images $u$ and $v$ is different if one permutes the reference image in the pair $(u, v)$. To make the problem invariant to such permutation, one replaces the functions $\tau_{u,s}$ and $\phi_{uv}$ by their symmetrical versions

$$\tau_s(\mathbf{x}) = \min(\tau_{u,s}(\mathbf{x}), \tau_{v,s}(\mathbf{x})), \tag{14}$$

$$\varphi_{uv}(\mathbf{x}, \mathbf{y}, s) = \min(\phi_{uv}(\mathbf{x}, \mathbf{y}, s), \phi_{vu}(\mathbf{x}, \mathbf{y}, s)). \tag{15}$$

# 3 Experiments

## 3.1 The Dissimilarity Measures

Among the dissimilarity measures suggested by Kervrann et al., we have selected three functions:

- The first one is given by

$$\phi^\rho_{uv}(\mathbf{x}, \mathbf{y}, s) = \sum_{\mathbf{t} \in W_s} ((u(\mathbf{x} + \mathbf{t}) - u_\rho(\mathbf{x})) - (v(\mathbf{y} + \mathbf{t}) - v_\rho(\mathbf{y})))^2, \tag{16}$$

  where $u_\rho = u * G_\rho$ and $v_\rho = v * G_\rho$ are images convolved with a Gaussian kernel $G_\rho$ with standard deviation $\rho$, which is less sensitive to local additive contrast changes between the two input images.

**Algorithm 1:** Kervrann et al. symmetric change detection algorithm.

**Input** $u, v$**:** The image pair.
**Input** $S$**:** The number of patch scales.
**Input** $\phi_{uv}$**:** The dissimilarity measure between patches.
**Input** $b$**:** The square neighborhood around $\mathbf{x}$.
**Input** $B$**:** The square search window related to $\mathbf{x}$.
**Input** $\varepsilon$**:** The number of false alarms threshold.
**Output** $H_\varepsilon(u, v)$**:** The multiscale change detection map.

**for** $s \leftarrow 1, \ldots, S$ **do**
  *Computation of the global thresholds*
  $\theta_{u,s} \leftarrow \frac{1}{|\Omega|} \sum_{\mathbf{x}\in\Omega} \min_{\mathbf{y}\in b(\mathbf{x})\setminus\{\mathbf{x}\}} \phi_{uu}(\mathbf{x}, \mathbf{y}, s)$
  $\theta_{v,s} \leftarrow \frac{1}{|\Omega|} \sum_{\mathbf{x}\in\Omega} \min_{\mathbf{y}\in b(\mathbf{x})\setminus\{\mathbf{x}\}} \phi_{vv}(\mathbf{x}, \mathbf{y}, s)$
  *Computation of the decision thresholds*
  **for** $\mathbf{x} \in \Omega$ **do**
    $\tau_{u,s}(\mathbf{x}) \leftarrow \max(\max_{\mathbf{y}\in b(\mathbf{x})\setminus\{\mathbf{x}\}} \phi_{uu}(\mathbf{x}, \mathbf{y}, s), \theta_{u,s})$
    $\tau_{v,s}(\mathbf{x}) \leftarrow \max(\max_{\mathbf{y}\in b(\mathbf{x})\setminus\{\mathbf{x}\}} \phi_{vv}(\mathbf{x}, \mathbf{y}, s), \theta_{v,s})$
    $\tau_s(\mathbf{x}) \leftarrow \min(\tau_{u,s}(\mathbf{x}), \tau_{v,s}(\mathbf{x}))$
  *Computation of the number of positive decisions*
  **for** $\mathbf{x} \in \Omega$ **do**
    $\varphi_{uv}(\mathbf{x}, \mathbf{y}, s) \leftarrow \min(\phi_{uv}(\mathbf{x}, \mathbf{y}, s), \phi_{vu}(\mathbf{x}, \mathbf{y}, s))$
    $F_s(\mathbf{x}) \leftarrow \sum_{\mathbf{y}\in B(\mathbf{x})} \mathbb{1}(\varphi_{uv}(\mathbf{x}, \mathbf{y}, s) \geq \tau_s(\mathbf{x}))$
  *Probability of positive detections under* $H_0$
  $P_{fa}(s) \leftarrow \frac{1}{|\Omega|} \sum_{\mathbf{x}\in\Omega} \exp(F_s(\mathbf{x}) - |B(\mathbf{x})|)$
*Computation of the Poisson law parameter*
$\lambda \leftarrow \sum_{s=1}^{S} P_{fa}(s)$
**for** $\mathbf{x} \in \Omega$ **do**
  *Computation of the number of positive detections*
  $k_D(\mathbf{x}) \leftarrow \sum_{s=1}^{S} \mathbb{1}(F_s(\mathbf{x}) = |B(\mathbf{x})|)$
  *Computation of the probability of false alarms*
  $P_{FA}(\mathbf{x}, F) \leftarrow 1 - \sum_{k=0}^{k_D(\mathbf{x})} \lambda^k \frac{e^{-\lambda}}{k!}$
*Computation of the uniform threshold to detect meaningful changes*
$\alpha \leftarrow \max\left(\frac{\varepsilon}{|\Omega|}, \inf_{\mathbf{x}\in\Omega} P_{FA}(\mathbf{x}, F)\right)$
*Computation of the change detection map*
**for** $\mathbf{x} \in \Omega$ **do**
  $H_\varepsilon(u, v)(\mathbf{x}) \leftarrow \mathbb{1}(P_{FA}(\mathbf{x}, F) \leq \alpha)$
**return** $H_\varepsilon(u, v)$

- The second one is

$$\phi_{uv}^{\text{mult}}(\mathbf{x},\mathbf{y},s)=\sum_{\mathbf{t}\in W_s}\left(u(\mathbf{x}+\mathbf{t})-\frac{u_\rho(\mathbf{x})}{v_\rho(\mathbf{y})}v(\mathbf{y}+\mathbf{t})\right)^2, \tag{17}$$

  which is invariant to multiplicative illumination changes.

- Finally, we select the function

$$\phi_{uv}^{\text{corr}}(\mathbf{x},\mathbf{y},s)=1-\frac{\sum_{\mathbf{t}\in W_s}u(\mathbf{x}+\mathbf{t})v(\mathbf{y}+\mathbf{t})}{(\sum_{\mathbf{t}\in W_s}u^2(\mathbf{x}+\mathbf{t})\times\sum_{\mathbf{t}\in W_s}v^2(\mathbf{y}+\mathbf{t}))^{1/2}}, \tag{18}$$

  which is a correlation measure mitigating magnitude scaling.

In addition, we introduce the measure denoted $\text{LIN}^2$ by Delon et al. [7]:

$$\phi_{uv}^{\text{LIN}^2}(\mathbf{x},\mathbf{y},s)=\max(U_s(\mathbf{x}),V_s(\mathbf{y}))\left(1-\frac{\sum_{\mathbf{t}\in W_s}u(\mathbf{x}+\mathbf{t})v(\mathbf{y}+\mathbf{t})}{U_s(\mathbf{x})V_s(\mathbf{y})}\right), \tag{19}$$

where $U_s(\mathbf{x})\triangleq\sum_{\mathbf{t}\in W_s}u^2(\mathbf{x}+\mathbf{t})$ and $V_s(\mathbf{x})\triangleq\sum_{\mathbf{t}\in W_s}v^2(\mathbf{y}+\mathbf{t})$. This measure is invariant to affine contrast changes, and different from the normalized cross-correlation in that it can distinguish flat patches from those containing edges.

## 3.2 Quantitative and Qualitative Results

To carry out our experiments, we used the ONERA satellite image pair dataset (OSCD) [4], composed of 24 Sentinel-2 orthorectified pairs from various locations. We measure performance in terms of precision, recall and $F1$ score, from the false positives, true positives, false negatives and true negatives computed pixel-wise, then summed over all the locations. To observe the influence of the main parameters i.e., $b\in[3\times3,5\times5,7\times7]$, $B\in[3\times3,5\times5,7\times7]$, $S\in[1,3,5,7]$ and the four dissimilarity measures on the performances, we combine them according to a Cartesian product so that 144 parameter configurations were computed per location. Results are shown in Table 2: for a given parameter, the reported recall, precision and $F1$ score correspond to the average values computed over all the other parameters. Although the parameter $B$ has little influence, performance depends mainly on the number of scales $S$ and the type of measure. We observe that the $\text{LIN}^2$ measure, which is invariant to affine contrast changes, yields the best scores. By applying the optimal parameters of each category, i.e. $B=3\times3$, $b=3\times3$, $S=7$ and $\phi^{\text{LIN}^2}$, one finds a recall of 31.72, a precision of 29.76 and a $\text{F}_1$ score of 30.71.

Qualitative and quantitative results are shown in Figures 1, 2, 3 and 4. Their change maps were estimated from the previously mentioned optimal set of parameters. We must emphasize that, as the method is applied in an unsupervised manner, a proportion of the detections are considered false alarms according to the ground truth, because they have no semantic relevance. Furthermore, some ground truths (see, e.g., the Beirut harbor on the top right of Figure 1) are represented by dense polygons while the real observable difference surfaces are more sparse and more similar to those of the estimated surfaces. That is why we can affirm that, most of the time, large-scale changes in cityscapes are globally well detected. This observation is not true when dealing with countryside images (see Figure 4), where the dissimilarity measures are not sufficiently invariant to attenuate the contrast changes due to the vegetation. In the case of Saclay, and contrary to the preceding figures taken in dry or even desert countries, there is noticeable strong seasonal change in the aspect of objects due to shadows in the cities and cultivation cycles. This points to the necessity of comparing images taken at similar seasons to reduce the number of false alarms (see Figure 5).

Image 1

Image 2

Ground truth

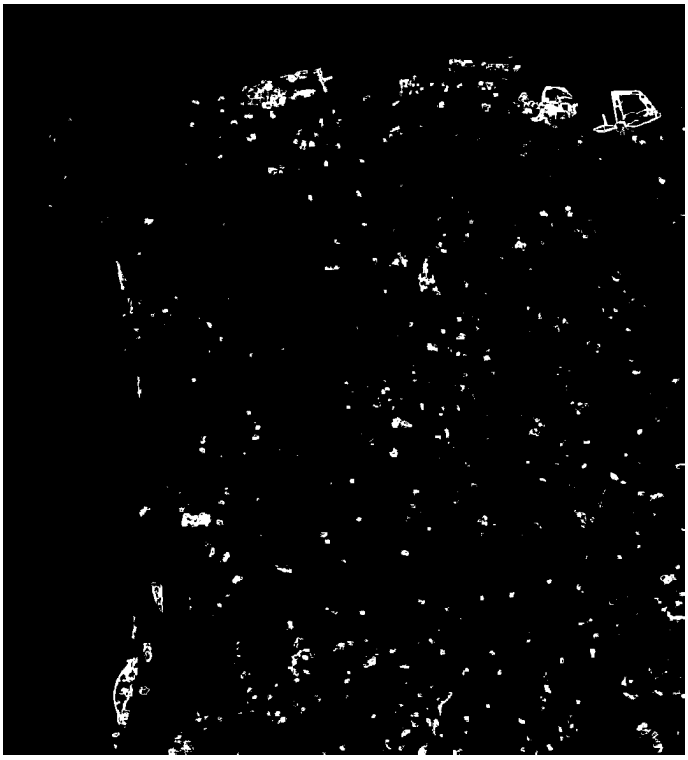

Estimated map

Figure 1: The Beirut pair. The large change areas are globally well located.

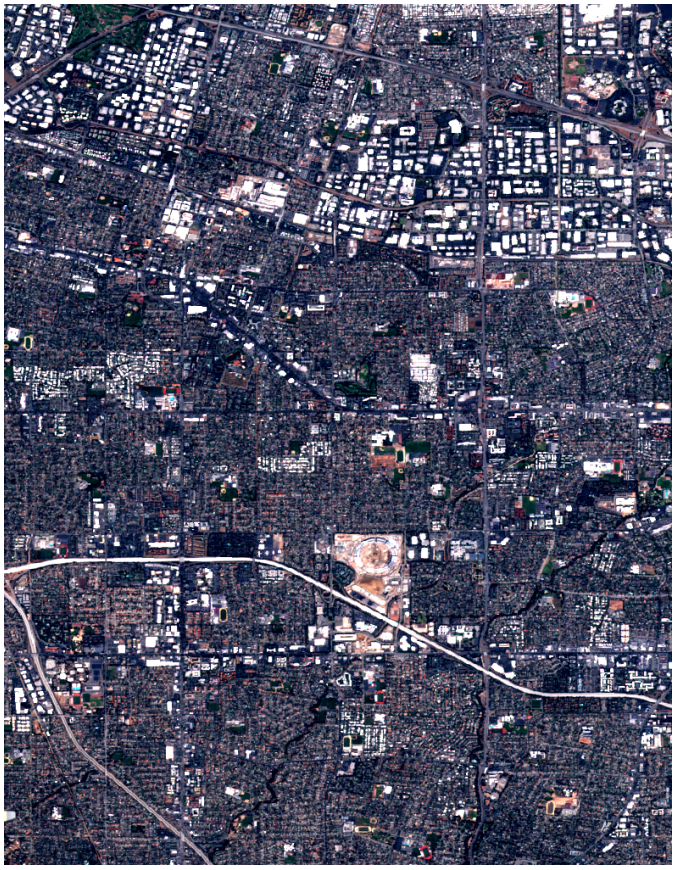

Image 1

Image 2

Ground truth

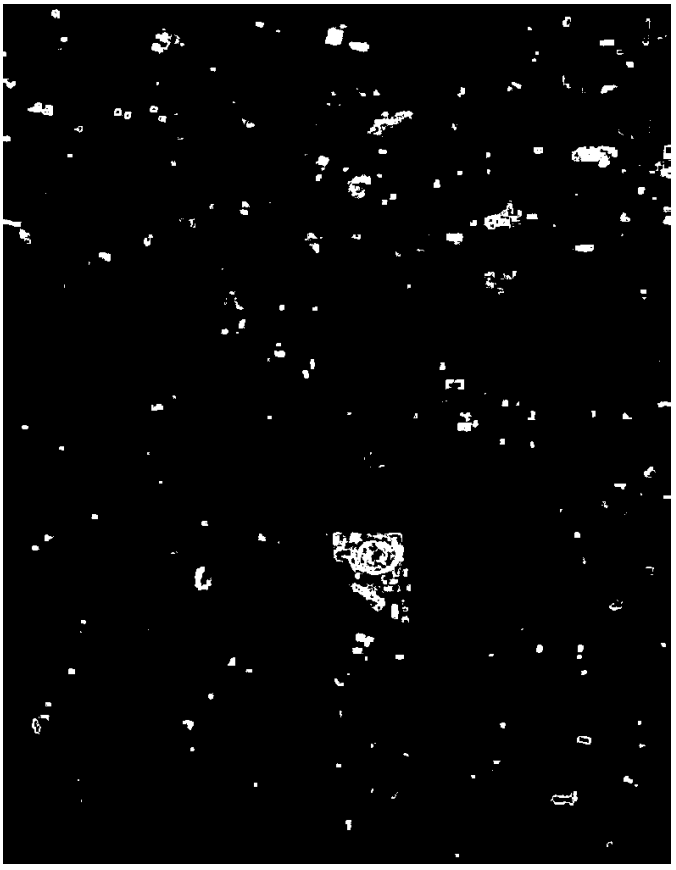

Estimated map

Figure 2: The Cupertino pair. The large change areas are globally well located.

Image 1

Image 2

Ground truth

Estimated map

Figure 3: The Las Vegas pair. Most of the large change areas are globally well located. However, as the dissimilarity metric is quite invariant to illumination changes, the large areas where only a contrast change happens (see e.g. the black area at the center of image 2) are under-estimated.

Image 1

Image 2

Ground truth

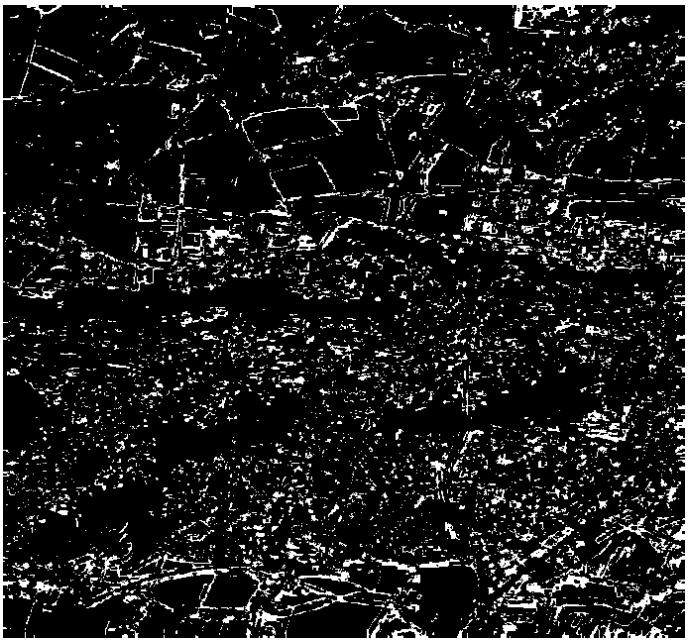

Estimated map

Figure 4: The Saclay pair. The change estimation totally fails in this pair: the large change areas are not located and a lot of false alarms occur in the countryside areas.

2018-08-11

2019-02-12

2019-08-11

2020-02-02

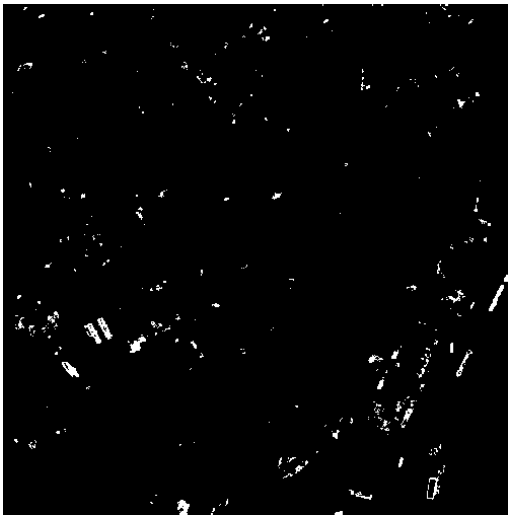

2018-08-11 vs. 2019-02-12

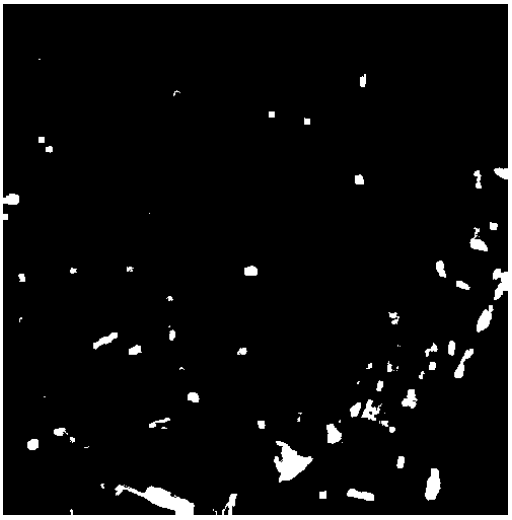

2018-08-11 vs. 2019-08-11

Figure 5: This example illustrates the importance of seasonality in image comparison: landscapes at dates 2018-08-11 and 2019-08-11, respectively 2019-02-12 and 2020-02-02, are strongly similar. Although the detection maps presented here are calculated from two different pairs, it is clear that the left map contains many false alarms in the form of small isolated regions, while the right map does not. In the first case, these false alarms are due to the variation in building shadows between February and August. In the second case, where both images were acquired in August, this phenomenon is not observed.

| Param. $B$ | Recall | Precision | $F_1$ score |
|---|---|---|---|
| $3 \times 3$ | 7.65 | 25.99 | 11.83 |
| $5 \times 5$ | 7.58 | 25.83 | 11.72 |
| $7 \times 7$ | 7.65 | 25.99 | 11.83 |

| Param. $b$ | Recall | Precision | $F_1$ score |
|---|---|---|---|
| $3 \times 3$ | 18.57 | 21.30 | 19.84 |
| $5 \times 5$ | 7.46 | 39.91 | 12.57 |
| $7 \times 7$ | 4.48 | 38.38 | 8.03 |

| Param. $S$ | Recall | Precision | $F_1$ score |
|---|---|---|---|
| 1 | 4.90 | 18.61 | 7.76 |
| 3 | 5.27 | 23.07 | 8.58 |
| 5 | 7.94 | 28.67 | 12.44 |
| 7 | 12.45 | 30.45 | 17.67 |

| Measure | Recall | Precision | $F_1$ score |
|---|---|---|---|
| $\phi^{\text{corr}}$ | 7.74 | 25.03 | 11.83 |
| $\phi^{\text{LIN}^2}$ | 10.62 | 30.14 | 15.71 |
| $\phi^{\text{mult}}$ | 7.05 | 27.16 | 11.20 |
| $\phi^{\rho}$ | 9.39 | 30.04 | 14.31 |

Table 2: Trends of the performances according to the main parameters of the algorithm. For a given parameter, the recall, precision and $F1$ score correspond to the average values computed over the Cartesian product of the other parameters.

# 4 Conclusion

In this paper, we investigated the symmetrical version of the change detector of Kervrann et al. [12]. We first theoretically described the algorithm by its equations, then by an explicit pseudo-code, and finally evaluated it on satellite image pairs. As the method is highly interpretable, false alarms as well as misses can be easily interpreted. Although the method was originally designed for video surveillance, its application to remote sensing imagery shows interesting and valid results in cityscapes. As the method is independent of the satellite technologies and of the spectral band, it could be integrated into any unsupervised first stage observation pipeline.

# Image Credits

All images come from the OSCD dataset [4] except those in Figure 5, which were produced by the authors.

# References

[1] A. Akhyar, M. Asyraf Zulkifley, J. Lee, T. Song, J. Han, C. Cho, S. Hyun, Y. Son, and B.-W. Hong, *Deep Artificial Intelligence Applications for Natural Disaster Management Systems: A Methodological Review*, Ecological Indicators, 163 (2024), p. 112067, https://doi.org/https://doi.org/10.1016/j.ecolind.2024.112067.

[2] M. H. Asad, M. M. Asim, M. N. M. Awan, and M. H. Yousaf, *Natural Disaster Damage Assessment Using Semantic Segmentation of UAV Imagery*, in International Conference on Robotics and Automation in Industry (ICRAI), 2023, pp. 1–7, https://doi.org/10.1109/ICRAI57502.2023.10089539.

[3] A. Buades, J. L. Lisani, and L. Rudin, *Adaptive Change Detection*, in 2009 16th International Conference on Systems, Signals and Image Processing, 2009, pp. 1–4, https://doi.org/10.1109/IWSSIP.2009.5367788.

[4] R. Caye Daudt, B. Le Saux, A. Boulch, and Y. Gousseau, *Urban Change Detection for Multispectral Earth Observation Using Convolutional Neural Networks*, in IEEE International Geoscience and Remote Sensing Symposium (IGARSS), 2018, https://doi.org/10.1109/IGARSS.2018.8518015.

[5] L. H. Y. Chen, *Poisson Approximation for Dependent Trials*, The Annals of Probability, 3 (1975), pp. 534–545, https://doi.org/10.1214/aop/1176996359.

[6] G. Cheng, Y. Huang, X. Li, S. Lyu, Z. Xu, Q. Zhao, and S. Xiang, *Change Detection Methods for Remote Sensing in the Last Decade: A Comprehensive Review*, 2023, https://doi.org/10.48550/arXiv.2305.05813.

[7] J. Delon and A. Desolneux, *Stabilization of Flicker-Like Effects in Image Sequences Through Local Contrast Correction*, SIAM Journal on Imaging Sciences, 3 (2010), pp. 703–734, https://doi.org/10.1137/090766371.

[8] S. Hafner, H. Fang, H. Azizpour, and Y. Ban, *Continuous Urban Change Detection from Satellite Image Time Series with Temporal Feature Refinement and Multi-Task Integration*, ArXiv, (2024), https://doi.org/10.48550/arXiv.2406.17458.

[9] H. He, J. Yan, D. Liang, Z. Sun, J. Li, and L. Wang, *Time-Series Land Cover Change Detection Using Deep Learning-Based Temporal Semantic Segmentation*, Remote Sensing of Environment, 305 (2024), p. 114101, https://doi.org/10.1016/j.rse.2024.114101.

[10] H. Jiang, M. Peng, Y. Zhong, H. Xie, Z. Hao, J. Lin, X. Ma, and X. g. Hu, *A Survey on Deep Learning-Based Change Detection from High-Resolution Remote Sensing Images*, Remote Sensing, 14 (2022), https://doi.org/10.3390/rs14071552.

[11] A. Kalogeras, D. Bormpoudakis, I. Tsardanidis, D. A. Loka, and C. Kontoes, *Monitoring Digestate Application on Agricultural Crops Using Sentinel-2 Satellite Imagery*, ArXiv, (2025), https://doi.org/10.48550/arXiv.2504.19996.

[12] C. Kervrann, J. Boulanger, T. Pécot, P. Pérez, and J. Salamero, *Multiscale NeighborhoodWise Decision Fusion for Redundancy Detection in Image Pairs*, Multiscale Modeling and Simulation, 9 (2011), pp. 1829–1865, https://doi.org/10.1137/100791786.

[13] M. O. Turkoglu, S. D'Aronco, G. Perich, F. Liebisch, C. Streit, K. Schindler, and J. D. Wegner, *Crop Mapping from Image Time Series: Deep Learning with Multi-Scale Label Hierarchies*, Remote Sensing of Environment, 264 (2021), p. 112603, https://doi.org/https://doi.org/10.1016/j.rse.2021.112603.

[14] C. Wu, L. Zhang, B. Du, H. Chen, J. Wang, and H. Zhong, *UNet-Like Remote Sensing Change Detection: A Review of Current Models and Research Directions*, IEEE Geoscience and Remote Sensing Magazine, 12 (2024), pp. 305–334, https://doi.org/10.1109/MGRS.2024.3412770.